PHYSICAL REVIEW C

NUCLEAR PHYSICS

THIRD SERIES, VOL 6, NO. 6 December 1972

Multipole Theory of Neutrino-Nuclear Reactions: Application to ^{12}C

H. Überall* and Bernhard A. Lamers
Department of Physics, The Catholic University of America, Washington, D. C. 20017†

and

James B. Langworthy and Francis J. Kelly
U. S. Naval Research Laboratory, Washington, D. C. 20390
(Received 22 May 1972)

The cross section for neutrino-induced nuclear reactions is presented in the form of a multipole expansion, appropriate for the excitation of nuclear levels of a definite spin and parity. The theory is then applied to the $T=1$ levels of ^{12}C, knowledge of their excitation cross sections being required for both low-energy ($E_\nu \leq 53$ MeV, with neutrinos from stopped muons) and high-energy ($E_\nu \sim$ GeV) neutrino experiments that use counters containing carbon. We take a phenomenological approach, determining the needed transition densities from fits to the measured form factors of these levels for the closely related electroexcitation process. While the low-energy cross section is dominated by the excitation of the 1^+ ground state of ^{12}N, the high-energy cross sections receive their largest contributions from both positive-parity spin-flip states and especially from the 1^- giant-resonance levels, with additional strength from 3^+ and 2^-, 4^- levels.

I. INTRODUCTION

The excitation of the $T_3 \neq 0$ analogs of $T=1$ levels of ^{12}C by neutrinos incident on a carbon target has been investigated theoretically previously. This includes the transition to the 1^+ ground state of ^{12}N, obtained in a shell-model calculation and normalized by the observed ^{12}N β decay,[1] as well as the excitation of the 1^- "isospin" (i) and the 0^-, 1^-, and 2^- "spin-isospin" (si) or "spin-flip" components of the giant resonance,[2,3] calculated using the generalized Goldhaber-Teller model[4] or the particle-hole model[5,6] of Gillet. In addition, theoretical studies of the transition to the nuclear continuum have been made,[7-10] and the differential cross section summed over excitation energies has been obtained by a sum rule.[11]

While the neutrino excitation of nuclear levels is an interesting subject *per se*, its understanding becomes equally important for all those neutrino-induced elementary-particle reactions where complex nuclei are present in the counters and/or the target material. Two different types of neutrino experiments may be considered, namely (a) experiments with neutrinos of energy $E_\nu \leq 53$ MeV from the decay of stopped muons,[12] which have been proposed[13] for high-intensity meson facilities such as LAMPF at Los Alamos, and (b) experiments with neutrinos in the GeV range, as obtained, e.g., at NAL, Batavia, Illinois. Most of the mentioned relevant cross-section calculations are based entirely on theoretical models, and it is well known that the particle-hole model, for example, predicts cross sections for electroexcitation (a process closely related to neutrino excitation) that exceed the measured ones by factors of up to four.[14] For the present purpose of obtaining neutrino cross sections for a ^{12}C target with the excitation of all known $T=1$ levels of ^{12}N,

$$\nu_e + {}^{12}C \rightarrow {}^{12}N^{(*)} + e^- \tag{1a}$$

or

$$\nu_\mu + {}^{12}\mathrm{C} \rightarrow {}^{12}\mathrm{N}^{(*)} + \mu^- \tag{1b}$$

(including the giant resonances and partly also the rest of the continuum of ^{12}N), we deemed it most reliable to follow a phenomenological approach, by obtaining fits to the measured electroexcitation form factors of the $T=1$ levels in ^{12}C with the help of the generalized Helm model,[15] and by then using the same model to predict the neutrino cross sections of the analog states in ^{12}N. By including the "photon points"[3] of the levels in our fits whenever these were measured, we endeavored to render our results partly model-independent and hence more reliable even for the low-energy neutrino experiments.

In order to carry out such a program[16] for ^{12}C, we found it advantageous to expand the general neutrino excitation formulas[4,5] in a multipole series, appropriate for the excitation of nuclear levels with a given spin and parity. These multipole formulas are derived in Sec. II in terms of reduced matrix elements. They are of general validity independently of any model, and they simplify upon the use of the Helm model. In Sec. III, we describe our determination of the Helm model parameters by a fit of the electroexcitation cross sections to the measured ^{12}C level form factors, and in Sec. IV, we present our predicted neutrino cross sections and the angular distributions of the produced leptons in Eqs. (1), both for low ($E_\nu \leq 120$ MeV) and for high ($E_\nu \leq 500$ MeV) neutrino energies.

II. MULTIPOLE NUCLEAR CROSS SECTIONS FOR NEUTRINOS

We consider the reactions

$$\nu_l + A_Z \rightarrow A^{(*)}_{Z+1} + l^- \tag{2a}$$

and

$$\bar{\nu}_l + A_Z \rightarrow A^{(*)}_{Z-1} + l^+ , \tag{2b}$$

where $l = e$ or μ, with nuclear states $|J_i, M_i\rangle$ of A_Z and $|J_f, M_f\rangle$ of $A_{Z\pm1}$. The nuclear recoil is $\vec{q} = \vec{\nu} - \vec{l}$ ($\vec{\nu}, \vec{l}$ being the momenta of ν_l, l), and the lepton energy is $E_l = \nu - \omega \pm m_e$, ω being the excitation energy of $A_{Z\pm1}$ measured from the ground state of A_Z (in atomic mass units, with m_e the electron mass). This gives for the reaction threshold

$$\nu_{\mathrm{thresh}} = \omega + m_l \mp m_e . \tag{3}$$

In the nonrelativistic[17] Hamiltonian

$$H = \langle \phi_p \psi_l | [G_V + G_A \vec{\sigma}\cdot\vec{\sigma}^N + G_P(\vec{q}/2m)\cdot\vec{\sigma}^N\gamma_4 + iG_M(\vec{q}/2m)\cdot(\vec{\sigma}\times\vec{\sigma}^N)](1+\gamma_5)/\sqrt{2}\,|\psi_\nu \phi_n\rangle , \tag{4}$$

with m the proton mass, we shall only retain the vector term with $G_V = 10^{-5} m^{-2} f_p(\Delta^2)$ and the axial vector, $G_A = -1.20\, G_V$, since we feel that the modest accuracy of present-day nuclear models, in particular of the Helm model used below, does not really warrant the inclusion of the small pseudoscalar (G_P) and weak magnetic (G_M) terms.[18] For the proton electromagnetic form factor $f_p(\Delta^2)$ (a function of $\Delta^2 = q^2 - \omega^2$) whose presence is suggested by the conserved-vector-current hypothesis, we took the empirical expression of Janssen.[3] The differential cross section of reactions (2) is then found as

$$\frac{d\sigma}{d\Omega_l} = \frac{lE_l}{4\pi^2}\frac{1}{\hat{J}_i^2}\sum_{M_i M_f}\{G_V^2(1+\hat{\nu}\cdot\hat{l})|\mathfrak{M}|^2 - 2G_V G_A[\mathrm{Re}\mathfrak{M}^*\vec{\mathfrak{M}}\cdot(\hat{\nu}+\hat{l}) \pm \mathrm{Im}\mathfrak{M}^*\vec{\mathfrak{M}}\cdot(\hat{\nu}\times\hat{l})]$$
$$+ G_A^2[2\,\mathrm{Re}\vec{\mathfrak{M}}^*\cdot\hat{\nu}\vec{\mathfrak{M}}\cdot\hat{l} + |\vec{\mathfrak{M}}|^2(1-\hat{\nu}\cdot\hat{l}) \mp i(\hat{\nu}-\hat{l})\cdot(\vec{\mathfrak{M}}^*\times\vec{\mathfrak{M}})]\}, \tag{5}$$

where $\hat{J}_i = (2J_i+1)^{1/2}$, $\hat{\nu} = \vec{\nu}/\nu$, $\hat{l} = \vec{l}/E_l$, and the nuclear transition matrix elements are

$$\mathfrak{M}(\vec{q}) = \left\langle J_f M_f \left| \sum_{i=1}^{A} e^{i\vec{q}\cdot\vec{r}_i}\tau_i^{\pm} \right| J_i M_i \right\rangle, \tag{6a}$$

$$\vec{\mathfrak{M}}(\vec{q}) = \left\langle J_f M_f \left| \sum_{i=1}^{A} e^{i\vec{q}\cdot\vec{r}_i}\vec{\sigma}^{(i)}\tau_i^{\pm} \right| J_i M_i \right\rangle, \tag{6b}$$

where $\tau^+ n = p$, $\tau^- p = n$. The Wigner-Eckart theorem in isospin relates these to the matrix elements

$$\mathfrak{M}'(\vec{q}) = \tfrac{1}{2}\left\langle J_f M_f \left| \sum_{i=1}^{A} e^{i\vec{q}\cdot\vec{r}_i}\tau_i^{\,3} \right| J_i M_i \right\rangle, \tag{7a}$$

$$\vec{\mathfrak{M}}'(\vec{q}) = \tfrac{1}{2}\left\langle J_f M_f \left| \sum_{i=1}^{A} e^{i\vec{q}\cdot\vec{r}_i}\vec{\sigma}^{(i)}\tau_i^{\,3} \right| J_i M_i \right\rangle, \tag{7b}$$

so that, e.g., for self-conjugate nuclei such as ^{12}C,

$$\mathfrak{M} = \mp\sqrt{2}\,\mathfrak{M}', \quad \vec{\mathfrak{M}} = \mp\sqrt{2}\,\vec{\mathfrak{M}}'. \tag{8}$$

These matrix elements may be written in the form

$$\mathfrak{M}'(\vec{q}) = \int d^3r\, e^{i\vec{q}\cdot\vec{r}}\rho(\vec{r}), \quad \vec{\mathfrak{M}}'(\vec{q}) = \int d^3r\, e^{i\vec{q}\cdot\vec{r}}\vec{\rho}(\vec{r}), \tag{9}$$

where the transition densities

$$\rho(\vec{r}) = \langle J_f M_f | \rho^{\mathrm{op}}(\vec{r}) | J_i M_i \rangle, \tag{10a}$$

$$\vec{\rho}(\vec{r}) = \langle J_f M_f | \vec{\rho}^{\mathrm{op}}(\vec{r}) | J_i M_i \rangle \tag{10b}$$

are the matrix elements of corresponding transition operators for which we perform a multipole expansion[19]:

$$\rho^{\mathrm{op}}(\vec{r}) = \tfrac{1}{2}\sum_{i=1}^{A}\delta(\vec{r}-\vec{r}_i)\tau_i^3 = \sum_{lm}\tilde{\rho}_{lm}(r)Y^*_{lm}(\hat{r}), \tag{11a}$$

$$\vec{\rho}^{\mathrm{op}}(\vec{r}) = \tfrac{1}{2}\sum_{i=1}^{A}\delta(\vec{r}-\vec{r}_i)\vec{\sigma}^{(i)}\tau_i^3 = \sum_{ll'm}\tilde{\rho}_{ll'm}(r)\vec{Y}^{m*}_{ll'}(\hat{r}). \tag{11b}$$

Using the Wigner-Eckart theorem in the form

$$\langle J_f M_f | O_{LM} | J_i M_i \rangle = \hat{J}_f^{-1}(J_i M_i, LM | J_f M_f)\langle J_f \| O_L \| J_i \rangle, \tag{12}$$

we may express the transition densities as

$$\rho(\vec{r}) = \hat{J}_f^{-1}\sum_{lm}(J_i M_i, lm | J_f M_f)\rho_l^{if}(r)Y^*_{lm}(\hat{r}), \tag{13a}$$

$$\vec{\rho}(\vec{r}) = \hat{J}_f^{-1}\sum_{ll'm}(J_i M_i, lm | J_f M_f)\rho_{ll'}^{if}(r)\vec{Y}^{m*}_{ll'}(\hat{r}) \tag{13b}$$

in terms of their reduced matrix elements (or multipole transition densities)

$$\rho_l^{if}(r) = \langle J_f \| \tilde{\rho}_l(r) \| J_i \rangle, \tag{14a}$$

$$\rho_{ll'}^{if}(r) = \langle J_f \| \tilde{\rho}_{ll'}(r) \| J_i \rangle. \tag{14b}$$

Inserting Eqs. (13) into Eqs. (9) leads to a multipole expansion of the transition matrix elements

$$\mathfrak{M}'(\vec{q}) = (4\pi/\hat{J}_f)\sum_{LM}(J_i M_i, LM | J_f M_f)I_L(q)Y^*_{LM}(\hat{q}), \tag{15a}$$

$$\vec{\mathfrak{M}}'(\vec{q}) = (4\pi/\hat{J}_f)\sum_{LL'M}(J_i M_i, LM | J_f M_f)I_{LL'}(q)\vec{Y}^{M*}_{LL'}(\hat{q}) \tag{15b}$$

in terms of the reduced transition multipole matrix elements

$$I_L(q) = i^L\int r^2 j_L(qr)\rho_L^{if}(r)dr, \tag{16a}$$

$$I_{LL'}(q) = i^{L'}\int r^2 j_{L'}(qr)\rho_{LL'}^{if}(r)dr \tag{16b}$$

which contain the nuclear physics of the problem.

Equations (15) may now be inserted in the cross section of Eq. (5), and the nuclear spin sums evaluated using standard Racah algebra. Using Eqs. (A-7h) and (A-8e) of Ref. 3, we find as the result of some

lengthy but straightforward calculations [for the case of Eq. (8)]:

$$\frac{d\sigma}{d\Omega_l}=\frac{2}{\pi}\frac{lE_l}{\hat{J}_i^2}\{G_V^2(1+\hat{\nu}\cdot\tilde{l})\sum_L|I_L(q)|^2$$
$$+2G_VG_A[\hat{q}\cdot(\hat{\nu}+\tilde{l})\sum_{LL'}(L0,10|L'0)\,\mathrm{Re}I_L^*(q)I_{LL'}(q)\pm\hat{q}\cdot(\hat{\nu}\times\tilde{l})\sum_{LL'}(L0,10|L'0)\,\mathrm{Im}I_L^*(q)I_{LL'}(q)]$$
$$+G_A^2[(1-\tfrac{1}{3}\hat{\nu}\cdot\tilde{l})\sum_{LL'}|I_{LL'}(q)|^2$$
$$\mp\sqrt{2}\,\hat{q}\cdot(\hat{\nu}-\tilde{l})\sum_{LL'L''}(-1)^L\hat{L}'\hat{L}''(L'0,L''0|10)W(L'L''11;1L)I_{LL'}^*(q)I_{LL''}(q)$$
$$+\sqrt{6}\,(\hat{\nu}\cdot\hat{q}\tilde{l}\cdot\hat{q}-\tfrac{1}{3}\hat{\nu}\cdot\tilde{l})\sum_{LL'L''}(-1)^L\hat{L}'\hat{L}''(L'0,L''0|20)W(L'L''11;2L)I_{LL'}^*(q)I_{LL''}(q)]\}. \quad (17)$$

This expression may be simplified by parity considerations, assuming transitions to nonoverlapping nuclear levels. With $P|J_j\rangle=\pi_j|J_j\rangle$, one has from Eqs. (7):

$$\mathfrak{M}'(-\vec{q})=\pi_f\pi_i\mathfrak{M}'(\vec{q}),\quad \vec{\mathfrak{M}}'(-\vec{q})=\pi_f\pi_i\vec{\mathfrak{M}}'(\vec{q}). \quad (18)$$

On the other hand, using the well-defined parities of $\vec{Y}_{LL'}^M(\hat{q})$ [Ref. 3, Eq. (A-2h)], one finds from Eqs. (15) and (18):

$$\pi_i\pi_f=(-1)^L,\quad \text{for } I_L \text{ terms ("longitudinal" or CL)},$$
$$=(-1)^L,\quad \text{for } I_{LL} \text{ terms ("transverse electric" or EL)},$$
$$=(-1)^{L+1},\quad \text{for } I_{LL+1} \text{ terms ("transverse magnetic" or ML)}, \quad (19)$$

employing for the multipoles the terminology of electroexcitation.[3] (Note that CL and EL transitions have the same selection rule and may be commonly called EL). This gives for the transitions of a given multipolarity and type a cross section from which the interference terms are absent:

$$(d\sigma/d\Omega_l)_{\mathrm{EL}}=(2lE_l/\pi\hat{J}_i^2)\{G_V^2(1+\hat{\nu}\cdot\tilde{l})|I_L(q)|^2$$
$$+G_A^2[(1-\tfrac{1}{3}\hat{\nu}\cdot\tilde{l})+(-1)^L\sqrt{6}\,(\hat{\nu}\cdot\hat{q}\tilde{l}\cdot\hat{q}-\tfrac{1}{3}\hat{\nu}\cdot\tilde{l})\hat{L}^2(L0,L0|20)W(LL11;2L)]|I_{LL}(q)|^2\}, \quad (20a)$$

$$(d\sigma/d\Omega_l)_{\mathrm{ML}}=(2lE_l/\pi\hat{J}_i^2)G_A^2[(1-\tfrac{1}{3}\hat{\nu}\cdot\tilde{l})\sum_{L'}{}'|I_{LL'}(q)|^2$$
$$+(-1)^L\sqrt{6}\,(\hat{\nu}\cdot\hat{q}\tilde{l}\cdot\hat{q}-\tfrac{1}{3}\hat{\nu}\cdot\tilde{l})\sum_{L'}{}'\sum_{L''}{}'\hat{L}'\hat{L}''(L'0,L''0|20)W(L'L''11;2L)I_{LL'}^*(q)I_{LL''}(q)], \quad (20b)$$

where $\sum_{L'}'$ means $\sum_{L'=L\pm1}$. This is our general result for the multipole cross section of neutrino-induced nuclear reactions in self-conjugate nuclei leading to isolated nuclear levels.

III. COMPARISON WITH ELECTROEXCITATION CROSS SECTIONS

The corresponding multipole electroexcitation cross section is well known[3]; it is (in Born approximation)

$$d\sigma/d\Omega=4\pi\sigma_M^{(1)}(\Delta^2/q^2)^2\{F_C^2(q)+(q^2/\Delta^2)[\tfrac{1}{2}+(q^2/\Delta^2)\tan^2\tfrac{1}{2}\vartheta]F_T^2(q)\}, \quad (21a)$$

the Mott cross section being

$$\sigma_M^{(1)}=(\alpha/2k_1)^2(\cos\tfrac{1}{2}\vartheta/\sin^2\tfrac{1}{2}\vartheta)^2, \quad (21b)$$

with $\alpha=1/137$, where now $\vec{q}=\vec{k}_i-\vec{k}_f$; $\vec{k}_{i,f}$ are the initial and final electron momenta, $\vartheta=\sphericalangle(\vec{k}_1,\vec{k}_2)$, and $\Delta^2=q^2-\bar{\omega}^2$, where $\bar{\omega}$ is the electroexcited level energy in A_Z (differing from the energy ω of the analog in $A_{Z\pm1}$ by the Coulomb energy shift). The "form factors"

$$F_C^2(q)=\hat{J}_i^{-2}\sum_L|\mathfrak{M}_L(q)|^2, \quad (22a)$$

$$F_T^2(q)=\hat{J}_i^{-2}\sum_L[|\mathfrak{T}_L^E(q)|^2+|\mathfrak{T}_L^M(q)|^2] \quad (22b)$$

are given in terms of reduced transition multipole matrix elements

$$\mathfrak{M}_L(q) = i^L \int r^2 j_L(qr) \rho_L^{if}(r) dr \tag{23a}$$

(longitudinal),

$$\mathcal{T}_L^E(q) = i^{L+1}[(L+1)^{1/2}/\hat{L}] \int r^2 j_{L-1}(qr) j_{LL-1}^{if}(r) dr$$

$$- i^{L+1}(L^{1/2}/\hat{L}) \int r^2 j_{L+1}(qr) j_{LL+1}^{if}(r) dr + i^L q \int r^2 j_L(qr) \mu_{LL}^{if}(r) dr \tag{23b}$$

(transverse electric), and

$$\mathcal{T}_L^M(q) = i^L \int r^2 j_L(qr) j_{LL}^{if}(r) dr$$

$$+ i^{L+1} q[(L+1)^{1/2}/\hat{L}] \int r^2 j_{L-1}(qr) \mu_{LL-1}^{if}(r) dr - i^{L+1} q(L^{1/2}/\hat{L}) \int r^2 j_{L+1}(qr) \mu_{LL+1}^{if}(r) dr \tag{23c}$$

(transverse magnetic). The multipole transition densities $\rho_L^{if}(r)$ of charge, $j_{LL'}^{if}(r)$ of current and $\mu_{LL'}^{if}(r)$ of magnetization[3] are closely related to those of Eqs. (14) that contribute to the neutrino reaction; in fact, for self-conjugate nuclei ($T=0$ in the ground state) such as ^{12}C, only the isospin-one part contributes in the transitions to $T=1$ levels considered by us, and the scalar densities $\rho_L^{if}(r)$ in Eqs. (16a) and (23a) become identical, while we get the relation

$$\rho_{LL'}^{if}(r) = \frac{2m}{\mu_p - \mu_n} \mu_{LL'}^{if}(r) \tag{24}$$

for the vector (spin) densities, $\mu_p - \mu_n = 4.70$ being the difference between the proton and neutron magnetic moments. Note that neutrino reactions then depend on the nuclear charge and magnetization densities only, while electroexcitation contains current densities in addition.

In the following analysis, we shall adopt expressions for the densities provided by the generalized Helm model,[3,15] which assumes essentially a distribution peaked at the "transition radius" R and smeared by a Gaussian convolution of width g. This leads, apart from a factor due to the surface smearing

$$f_g(q) = e^{-g^2 q^2/2} \tag{25}$$

which all the form factors acquire, to the densities

$$\rho_L^{if}(r) = \hat{J}_i i^{-L} \beta_L r^{-2} \delta(r - R), \tag{26a}$$

$$\rho_{LL'}^{if}(r) = \hat{J}_i i^{-L'} \bar{\gamma}_{LL'} r^{-2} \delta(r - \bar{R}), \tag{26b}$$

where

$$\bar{\gamma}_{LL'} = \gamma_{LL'}/(\mu_p - \mu_n), \tag{27}$$

β_L and $\gamma_{LL'}$ ($\bar{\gamma}_{LL'}$) being strength parameters for transition charge and magnetization (spin) density. In this model, the reduced matrix elements become

$$I_L(q) = \hat{J}_i \beta_L f_g(q) j_L(qR), \tag{28a}$$

$$I_{LL'}(q) = \hat{J}_i \bar{\gamma}_{LL'} f_{\bar{g}}(q) j_{L'}(q\bar{R}) \tag{28b}$$

for neutrino reactions (allowing for different radial and surface parameters R, g and $\bar{R}, \bar{g}$ for charge and spin transitions, respectively), and

$$\mathfrak{M}_L(q) = \hat{J}_i \beta_L f_g(q) j_L(qr), \tag{29a}$$

$$\mathcal{T}_L^E(q) = \hat{J}_i \{[(L+1)/L]^{1/2} \beta_L (\bar{\omega}/q) f_g(q) j_L(qr) + \gamma_{LL}(q/2m) f_{\bar{g}}(q) j_L(q\bar{R})\}, \tag{29b}$$

$$\mathcal{T}_L^M(q) = -\hat{J}_i (q/2m) f_{\bar{g}}(q) \{(L^{1/2}/\hat{L}) \gamma_{LL+1} j_{L+1}(q\bar{R}) + [(L+1)/\hat{L}]^{1/2} \gamma_{LL-1} j_{L-1}(q\bar{R})\} \tag{29c}$$

for electroexcitation. In the latter case, the charge and electric current transitions are related by the Siegert theorem (hence the same parameter β_L), while no current contribution to the magnetic transitions was assumed. This seems quite justified for our purposes in view of the fact that the same assumption led to excellent agreement in comparisons of $M1$ and β analog transitions for self-conjugate $4N$ nuclei in the p and sd shells.[20] The negligibility of current compared to spin transition strength is made possible essentially by the fact that in the electromagnetic reaction, the spin term is enhanced over the current term by the large factor $\mu_p - \mu_n = 4.70$, while that factor is not present in the weak reaction, so that any error committed by the neglect of the current term in fitting the electron scattering form factor is reduced to 20% when the results of the fit are used for predicting weak cross sections.

We have employed Eqs. (22) and (29) for a fit to the electron scattering form factors of the $T=1$ levels of ^{12}C as measured by the Orsay[21] and Sendai[22] groups for values of q up to 530 MeV/c, in order to determine the parameters $R, g, \bar{R}, \bar{g}$, and $\beta_L, \gamma_{LL'}$ of each level. In addition, the "photon points" of the form factors, whenever available,[23] have been used for the fits also, in order to make the low-energy results more reliable and less model-dependent.

In Table I, we present the results of our fits for all $T=1$ bound and giant resonance levels in ^{12}C as observed in electroexcitation,[21,22] and in other experiments as compiled earlier by Segel *et al.*[23] Due to the similarity of electron- and neutrino-excitation matrix elements, all states observed in one process should also be seen in the other, with the exception of 0^- states that electrons do not excite. These states, however, may be taken from the particle-hole model: The calculation of Gillet[24] predicts two such levels at 24.9 and 34.0 MeV, respectively, and their (relatively small) neutrino cross sections have been calculated previously.[5,6]

The first column of Table I labels the levels, the second gives their excitation energy $\bar{\omega}$ in ^{12}C and the energy ω of the analogs in ^{12}N as measured from the ^{12}C ground state (with tentative identifications of known ^{12}N levels[25]). The third column gives spin and parity of the level, the fourth the character ($\sigma = E, M$) and multipolarity L of the transition together with an indication (s) of predominantly electric spin-flip states, or the SU_4 character (i: isospin, or si: spin-isospin[2,3]) for the giant-resonance states. The following columns present the parameters from our fits: note that the surface parameter was taken as $g = \bar{g} = 0.77$ F throughout. The only place where its value could be determined was in level No. 1 where

TABLE I. Parameters of $T=1$ levels in ^{12}C obtained by a fit of the generalized Helm model (Ref. 15) to the observed electroexcitation form factors (Refs. 21 and 22). We always fit with $g = \bar{g} = 0.77$ F.

Level No.	$\bar{\omega}$ (ω) in MeV	J^π	σL	R, F	β_L	$\bar{R}$, F	γ_{LL}	γ_{LL-1}	γ_{LL+1}	Reference
1	15.11 (17.34)	1^+	$M1$	···	···	2.24	···	0.97	0	a, b, c, d
2	16.11 (18.31)	2^+	$E2$, s	2.60	0.165	2.60	1.290	···	···	c, e
3	16.58 (18.54)	2^-	$M2$	···	···	2.82	···	0.65	−2.01	c, f
4	17.23 (18.99)	1^-	$E1$	1.70	0.092	1.70	0.247	···	···	c, f, g
5	17.77 (19.34)	0^+	CO			See text				f
6	18.15 (19.69)	1^-	$E1$, s	···	0	3.47	0.812	···	···	c
7	18.72 (20.49)	3^-	$E3$	2.85	0.315	···	0	···	···	c, f, h
8	18.81 (20.61)	2^+	$E2$	2.67	0.037	2.67	0.019	···	···	b, f
9	19.2 (20.9)	1^-	$E1$, s	2.08	0.048	2.08	0.338	···	···	f
10	19.4 (21.1)	2^-	$M2$, si	···	···	2.97	···	1.47	−0.99	c, h
11	19.6 (21.3)	4^-	$M4$	···	···	2.82	···	2.68	2.59	c, h
12	20.0 (21.7)	2^+	$E2$, s	2.50	0.123	2.50	0.421	···	···	c
13	20.6 (22.3)	3^+	$M3$	···	···	2.40	···	0.72	2.22	c
14	21.6 (23.3)	3^-	$E3$	2.82	0.243	2.82	0.700	···	···	c
15	22.0 (23.7)	1^-	$E1$, i	2.50	0.253	···	0	···	···	c
16	22.7 (24.4)	1^-	$E1$, si	···	0	2.60	0.829	···	···	c
17	23.8 (25.5)	1^-	$E1$, i	2.50	0.207	···	0	···	···	c
18	21–26 (23–29)	1^-	$E1$	2.08	0.438	2.08	2.230	···	···	c
19	21–37 (23–39)	1^-	$E1$	2.08	0.720	2.08	3.860	···	···	c
20	24.9 (26.6)	0^-	···, si			See text				i
21	25.5 (27.2)	3^-	$E3$	···	···	···	···	···	···	c
22	34.0 (35.7)	0^-	···			See text				i

[a] Reference 15.
[b] Reference 21.
[c] Reference 22.
[d] Reference 27.
[e] Reference 28.
[f] Reference 23.
[g] Reference 30.
[h] Reference 34.
[i] References 5, 6.

two successive diffraction peaks were measured in the form factor, and this value was retained for all the other levels. The last column lists the experimental reference used for the fits.

A short discussion of our fitting procedure follows, together with representative figures.

(1) 15.11 MeV, 1^+ level: The fit achieved with the parameters of Table I is shown in Fig. 1, with experimental points from Refs. 21 and especially 22. The inset to this figure presents the low-q portion of the fit, with points from[26] Ref. 15. The measured photon point[27] is located at $(4\pi/Z^2) \times (F_T/\bar{\omega})^2 = 2.6 \times 10^{-3}$ F^2, and is fitted by our model quite well.

(2) 16.11 MeV, 2^+ level: This is predominantly an electric spin-flip level,[28] with a photon point at $(4\pi/Z^2)(F_T/\bar{\omega})^2 = 1.94 \times 10^{-5}$ F^2. We fitted to this point and to the form factor data of Fig. 8 of Ref. 22.

(3) 16.58 MeV, 2^- level: Figure 2 presents our fit to the measured data[22]; the two-peak structure of this form factor does not represent successive diffraction peaks, but a destructive interference pattern of the two magnetic terms of Eq. (29c). Only a small upper limit is known[23] for the photon point, $(4\pi/Z^2)(F_T/\bar{\omega})^2 < 3 \times 10^{-5}$ F^2, and the value from our model (6×10^{-6} F^2) falls within this range.

(4) 17.23 MeV, 1^- level: Proca[29,21] sees here a strongly excited level, while Lightbody[30] and Yamaguchi[22] find only a weak one. Since the latter two measurements agree with each other, we adopted their data (Yamaguchi does not present them as a form factor, so that we had to read them off his published excitation spectrum). The measured photon point,[23] $(4\pi/Z^2)(F_T/\bar{\omega})^2 = 1.9 \times 10^{-3}$ F^2, was also taken into account by us.

(5) 17.77 MeV, 0^+ level: This monopole state is only mentioned by Segel[23] and has not been directly observed in the electroexcitation experiments. We therefore decided to calculate its excitation strength with the breathing-mode model,[31] in order to have at least theoretical information on it. This model predicts the form factor

$$I_0(q) \equiv F_C(q) = r_{\rm rms}^{-1}(8\pi m A\bar{\omega})^{-1/2} q[dF(q)/dq] \qquad (30a)$$

in terms of the ground-state form factor, for which the harmonic-oscillator result is applicable[32]:

$$F(q) = Z\{1 - \tfrac{1}{2}[\alpha q^2 a_0^2/(2+3\alpha)]\} e^{-q^2 a_0^2/4}, \qquad (30b)$$

with $\alpha = \frac{1}{3}(Z-2) = \frac{4}{3}$, and

$$a_0[\tfrac{3}{2}(2+5\alpha)/(2+3\alpha)]^{1/2} = r_{\rm rms} = 2.40 \text{ F}. \qquad (30c)$$

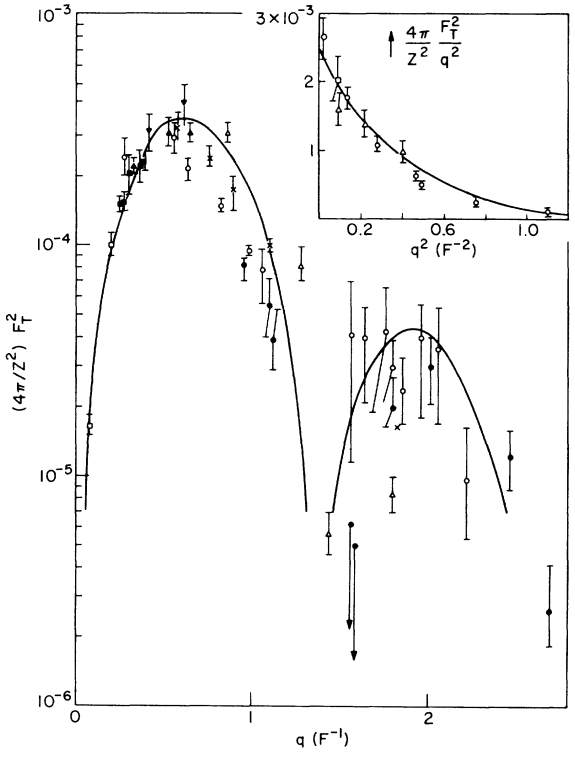

FIG. 1. Helm model fit to the form factor of the 15.11-MeV, 1^+ level in ^{12}C. Data from Yamaguchi (Ref. 22) and Rosen (Ref. 15).

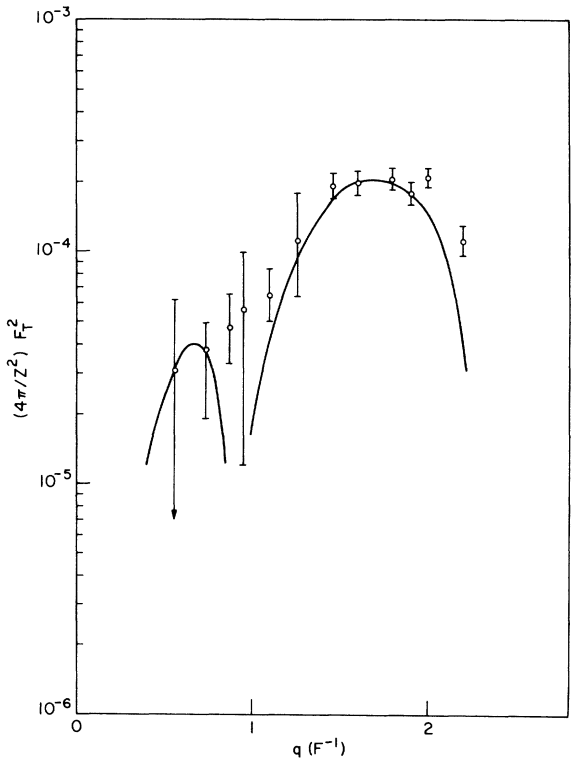

FIG. 2. Helm model fit to the form factor of the 16.58-MeV, 2^- level in ^{12}C. Data from Yamaguchi (Ref. 22).

It is known that, while the breathing model gives a good description of observed form factors, its absolute predicted magnitudes are too high by large factors.[33] Indeed when comparing the prediction of Eq. (30a) with Yamaguchi's[22] electroexcitation spectrum for $F_L^2(q)$, there seems to be indication of a small state at 17.77 MeV but with only about 2%, or at most 5%, of the intensity given by the breathing model.

(6) 18.15 MeV, 1^- level: This is observed by Yamaguchi[22] as a pure electric spin-flip level, hence is not contained in Segel's[23] low-energy data.

(7) 18.72 MeV, 3^- level: This state is listed by Segel,[23] but no photon point was measured. Yamaguchi[22] finds it purely longitudinal.

(8) 18.81 MeV, 2^+ level: This small state is not clearly seen by Yamaguchi.[22] We fitted to the photon point of Segel,[23] $(4\pi/Z^2)(F_T/\bar{\omega})^2 = 2.2\times10^{-5}$ F^2, and to the form factor of Proca.[21]

(9) 19.2 MeV, 1^- level: This state, together with the two following levels, is part of the experimentally unresolved "19-MeV complex" which also includes the

(10) 19.4 MeV, 2^- level, and the

(11) 19.6 MeV, 4^- level: They shall here be discussed together. The photon point of Segel[23] for the 1^- level, $(4\pi/Z^2)(F_T/\bar{\omega})^2 = 2.26\times10^{-3}$ F^2, was used to determine its Helm parameter β_1. The total complex, shown in Fig. 3 (transverse form factor), could be fitted relatively easily by the 2^- and 4^- states as shown (dotted curve). The lacking portion around $q \sim 1.0$ F^{-1} was then made up by the 1^- level whose γ_{11} parameter was thus determined. The same model was also found to provide a very good fit to the data published by Donnelly[34] that contain both transverse and longitudinal components, and include the 3^- state at 18.72 MeV as well.

(12) 20.0 MeV, 2^+ level: The longitudinal form factor of this state was fitted to Yamaguchi's[22] data, the transverse form factor to the calculation of Boyarkina (theoretical 23.9-MeV level) as quoted by Yamaguchi.

(13) 20.6 MeV, 3^+ level: The spin assignment was suggested for this state by Yamaguchi,[22] and we have fitted his transverse form factor.

(14) 21.6 MeV, 3^- level: This state besides the 0^+ state discussed earlier, presents the largest uncertainty in our analysis. It was seen as a weakly excited level in Yamaguchi's[22] electron spectra (both longitudinal and transverse), with a possible assignment of 2^+ or 3^-; the latter choice was suggested by comparison with a theoretical prediction,[35] rather than by a theoretical fit to a measured form factor. For our purpose, the form factors were extracted from Yamaguchi's electron spectra and fitted by the Helm model, which was

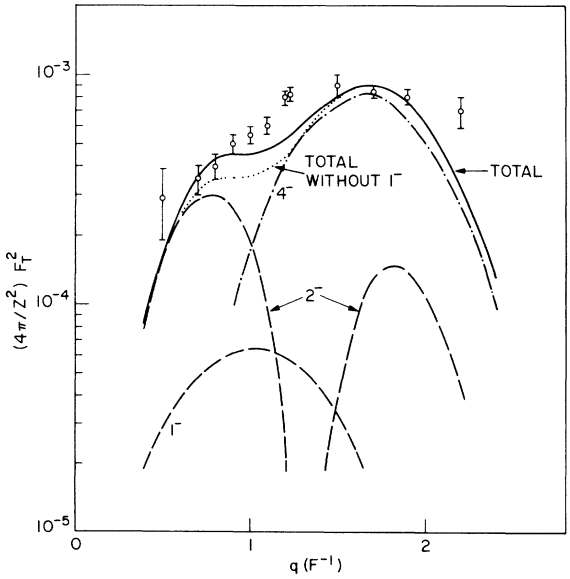

FIG. 3. Composite transverse form factor of the "19-MeV complex" containing 1^-, 2^-, and 4^- levels, and Helm model fit. Data from Yamaguchi (Ref. 22).

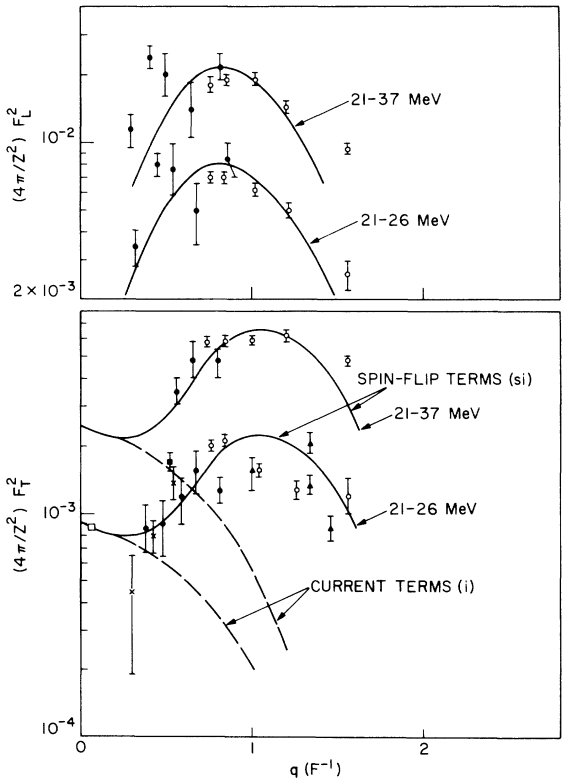

FIG. 4. Longitudinal and transverse form factor fits to Yamaguchi's (Ref. 22) data integrated over the 21–26-MeV and 21–37-MeV regions of excitation.

only possible within large error limits (up to perhaps a factor of 2).

(15) 22.0 MeV, 1^- level: This is a (purely longitudinal) isospin (i) component of the giant electric dipole resonance. Data of Yamaguchi[22] were fit.

(16) 22.7 MeV, 1^- level: This is the (purely transverse) spin-isospin (si) component of the giant electric dipole resonance; our fit is based on Yamaguchi's[22] data.

(17) 23.8 MeV, 1^- level: This is another purely longitudinal member of the giant electric dipole resonance, representing with the 22.0-MeV level a collective isospin vibration split into two levels. Yamaguchi's[22] data were fitted, and the summed isospin strength of the two i states gives with our fit a photon point value of $(4\pi/Z^2)(F_T/\bar{\omega})^2 = 5.3\times10^{-2}$ F^2 that compares reasonably well with the experimental value 6.0×10^{-2} F^2 of Bezic[36] as quoted by Yamaguchi.

(18) Summed (21–26 MeV) 1^- levels: Due to a large underlying continuum, Yamaguchi[22] does not present the individual form factors of levels above 24 MeV (such as the 25.5 MeV, 1^- state or the 29.0-MeV state), but only the integrated strength over the 21–26 MeV region, i.e., including the three preceding levels. We have fitted this composite as a 1^- excitation (Fig. 4), where for the transverse squared form factor, the current and spin contributions were added incoherently. This leads to the famous "dip"[3] in the integrated 1^- cross section separating the i and si terms. The photon point value $(4\pi/Z^2)(F_T/\bar{\omega})^2 = 6.3\times10^{-2}$ F^2 is again fitted to the Bezic[36] value as quoted by Yamaguchi.

(19) Summed (21–37 MeV) 1^- levels: This composite was fitted as the preceding, with results shown in Fig. 4 also.

(20) 24.9 MeV, 0^- level: This excitation cannot be seen in electron scattering, and the neutrino cross section will be taken from a particle-hole calculation.[5,6]

(21) 25.5 MeV, 3^- level: Yamaguchi[22] sees here at large values of q a state rising above the 1^- level, attributable to a predicted 3^- state. We found it impossible to extract any form factor values from his electron spectra, and were thus obliged to disregard this level.

(22) 34.0 MeV, 0^- level: The same remarks as for the 24.9 MeV, 0^- level apply here.

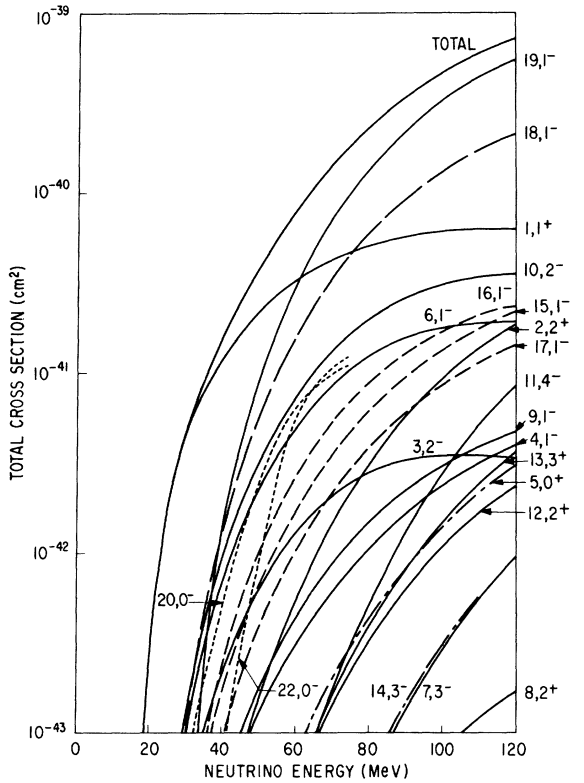

FIG. 5. Calculated ν_e cross section for excitation of ^{12}N levels in the range of low neutrino energies. States are labeled as in Table I. Dashed curves are included in the composite state No. 19; dash-dot curves are uncertain. Dotted cross sections (0^- levels) are taken from Ref. 6. Total does not include the dashed and the dotted curves.

IV. NEUTRINO CROSS SECTIONS

Using the Helm model parameters of Table I in the reduced matrix elements of Eqs. (28), we have calculated neutrino cross sections for reactions (1a) and (1b) from the formulas of Eqs. (20). We shall first consider low-energy cross sections ($E_\nu \leq 120$ MeV) for which only reaction (1a) is important; knowledge of this process is needed in the proposed stopped-muon source neutrino experiment.[13] Figure 5 presents the calculated total cross sections in this energy range; the excited ^{12}N states are labeled as in Table I. It is seen that below 60 MeV, it is one state that dominates the neutrino cross section, namely the ^{12}N ground-state (the analog of the 15.11 MeV, 1^+ state in ^{12}C). Only above this energy, the giant $E1$ states dominate the picture, i.e., mostly the $E1$ composite No. 19. The dashed curves designate $E1$ states included in No. 19, i.e., the composite No. 18 and the individual levels Nos. 15–17. Of the individual levels, the strongest one is actually No. 10, the 2^- member of the "19-MeV complex," and No. 6, an $E1$ spin-flip level. We have also entered as dotted curves the two 0^- levels Nos. 20 and 22, taken from the model calculation of Ref. 6; their strength is thus likely to be overestimated, perhaps by a factor of 2. The two states that are

most uncertain in our calculation (dash-dot) are No. 14 (3^-) and No. 5 (the 0^+ state, for which we multiplied the breathing mode result by 0.05); they are small in the low-energy region, however. The total cross section shown in Fig. 5 does not include the dashed and the dotted curves.

We may compare our semiempirical cross sections with those of the particle-hole model. Yamaguchi[22] has identified the states observed by him with those of the particle-hole model; the latter are listed in Table II in terms of their dominant configuration, together with the labels of Ref. 6. They are identified with the states of the present labeling, some of which being split up into several components experimentally. The reduction factors for going from particle-hole theory to phenomenological cross sections at $E_\nu = 60$ MeV (comparing with Fig. 2 of Ref. 6) are roughly 0.5, except for the 2^- level of the 19-MeV complex which is reduced by about 0.1.

It may be worthwhile noting that all these states, except for the ^{12}N ground state at $\omega = 17.34$ MeV, may decay by proton emission since the proton threshold lies by only 0.595 MeV above the ^{12}N ground state.

In Figs. 6 and 7, the angular distribution of the emitted electrons with respect to the incident neutrino direction are plotted *versus* the cosine of the electron angle for the most prominent or otherwise interesting states. Figure 6 presents the magnetic states: (a) the 1^+ state (No. 1), (b) the 2^- state (No. 10) (No. 3 having a similar angular distribution), and (c) the 4^- state (No. 11) [with a similar angular distribution of the 3^+ state (No. 13)]. One sees that while at low neutrino energies the electron always tends to emerge backward, at higher energies (~100 MeV) it will be emitted more in the forward direction for the $M1$ transition,[37] less so for $M2$, and it will still go backward for $M3$ and $M4$, due to the higher q dependence near threshold of the higher multipoles, favoring larger values of q and hence backward emission.

Figure 7 shows the angular distributions of the electric states: (a) the 0^+ state (No. 5), (b) the 1^- isospin state (No. 15, with No. 17 being similar), (c) the composite state No. 18 (with Nos. 19, 6 and the 1^- si state No. 16 being similar), (d) the 2^+ state (No. 2). Again, a backward shift takes place for the higher multipolarities; while the electron in the $E1$ (i) transition is still mainly forward, the $E1$ (si) transition tends to produce backward electrons due to its higher power of q, and the $E2$ and $E3$ transitions even more so. The 0^+ state has a characteristically different angular distribution.

All angular distributions in Figs. 6 and 7 were normalized to unity at 90° electron angles. We note that, as seen from Eqs. (20a), the angular distribution will be zero (for $E_l \gg m_l$) at 180° for electric states which have no spin transitions. This is exemplified by states Nos. 5, 7, 15, and 17.

The high-energy integrated cross sections ($E_\nu \leq 500$ MeV) are presented in Figs. 8(a) for created electrons, 8(b) for muons; they remain practically flat for higher energies (our calculations reach up to 2000 MeV). It is clear that in this domain, the giant $E1$ states dominate the neutrino cross section, especially those integrated over the continuum (No. 19 or 18), but also the individual $E1$ levels (Nos. 6, 15–17). The positive-parity spin-flip states (Nos. 1 and 2) still are very large, as well as the 2^- and 4^- states (Nos. 10 and 11) of the "19-MeV complex," which was to be expected. Another state, however, which also contributes noticeably at large E_ν is the 3^+ state No. 13. The 0^- state cross sections were again taken from previous calculations (Ref. 5). The "total" curve does not include the dashed and the dotted curves.

Comparing with the particle-hole results, Fig. 3 of Ref. 5, we find as shown in Table II that phenomenologically, the giant resonance $E1$ states

TABLE II. Identification of present states with particle-hole states, and approximate empirical reduction factor of neutrino cross sections at $E_\nu = 60$ MeV and $E_\nu = 1200$ MeV.

J^π	Dominant configuration	Reference 6 label	Present label	Reduction factor $E_\nu = 60$ MeV	Reduction factor $E_\nu = 1200$ MeV
1^-	$2s_{1/2}(1p_{3/2})^{-1}$	1	6	0.6	0.25
1^-i	$1d_{5/2}(1p_{3/2})^{-1}$	2	15, 17 (18)	0.6	0.8
1^-si	$1d_{3/2}(1p_{3/2})^{-1}$	3	16 (18)	0.4	1.0
2^-	$2s_{1/2}(1p_{3/2})^{-1}$	7	3	0.4	0.2
2^-	$1d_{5/2}(1p_{3/2})^{-1}$	8	10	0.1	0.2

at, e.g., $E_\nu = 1200$ MeV are hardly reduced at all, while the separate 1^- state and the 2^- states are reduced by factors of approximately 0.2. Figures 9 and 10 present typical angular distributions of the emitted electrons corresponding to the reaction (1a). Figures 9(a) and 9(b) show the angular distributions at 160, 300, and 500 MeV for the $M1$ state No. 1 and the $M3$ state No. 13, respectively, indicating the relative backward shift for the higher multipolarities, and relative forward shift for the higher energies. In Fig.

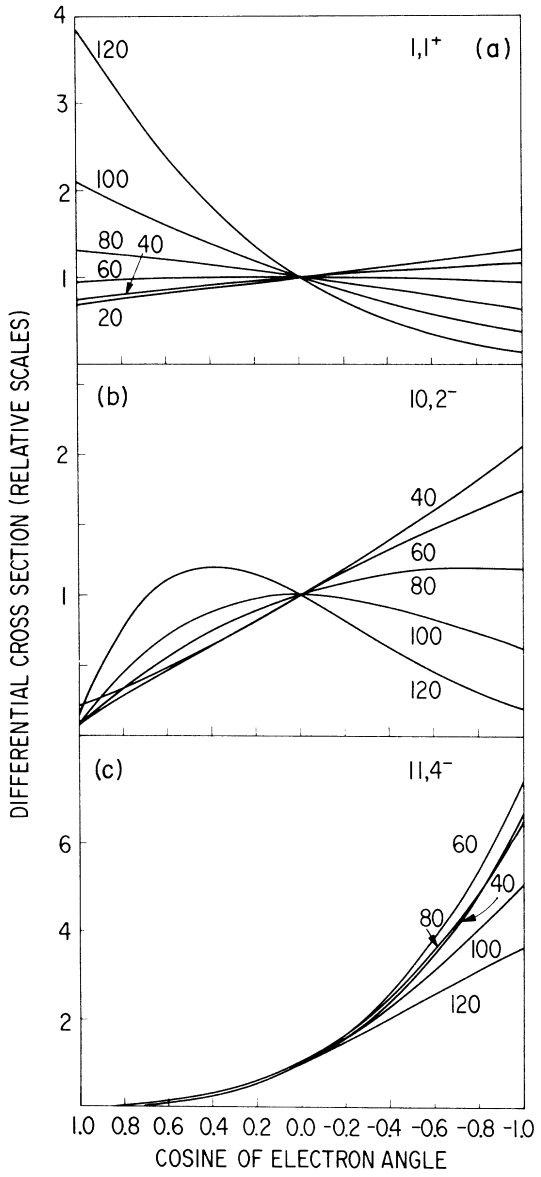

FIG. 6. Angular distributions of electrons emitted in reaction (1a) for magnetic states: (a) 1^+ (No. 1), (b) 2^- (No. 10), (c) 4^- (No. 11). Curves are labeled by the neutrino energy E_ν(in MeV).

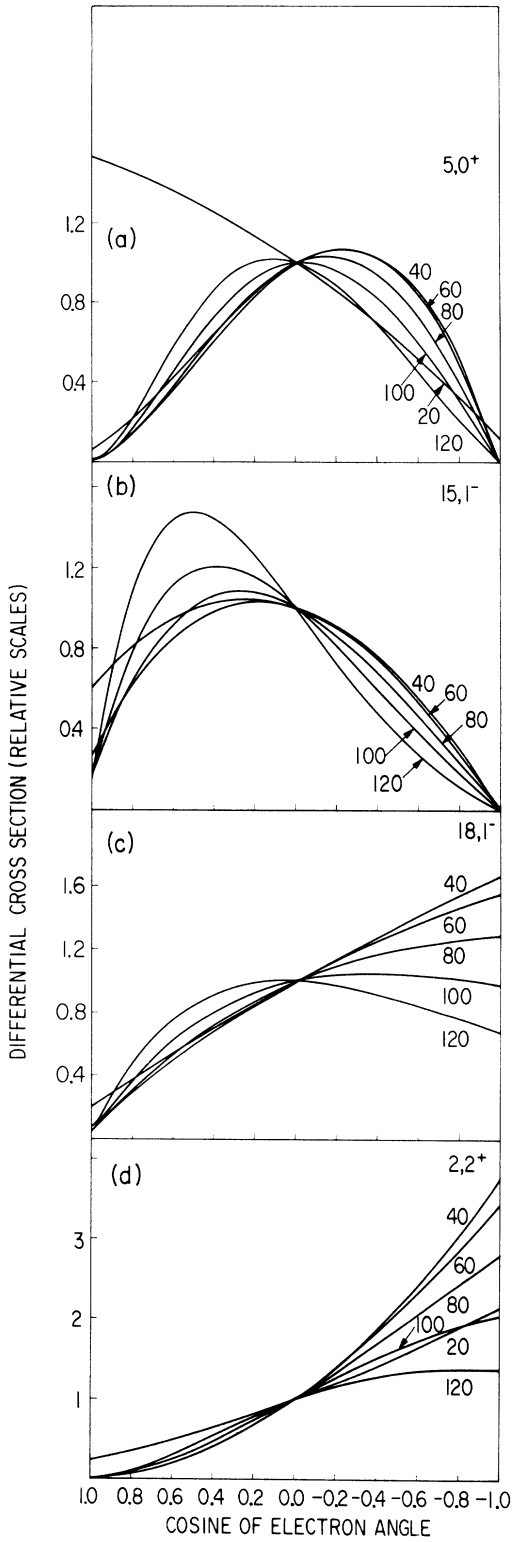

FIG. 7. Angular distributions for electrons emitted in reaction (1a) for electric states: (a) 0^+ (No. 5), (b) 1^- i (No. 15), (c) 1^- (No. 18), (d) 2^+ (No. 2). Curves are labeled by the neutrino energy (in MeV).

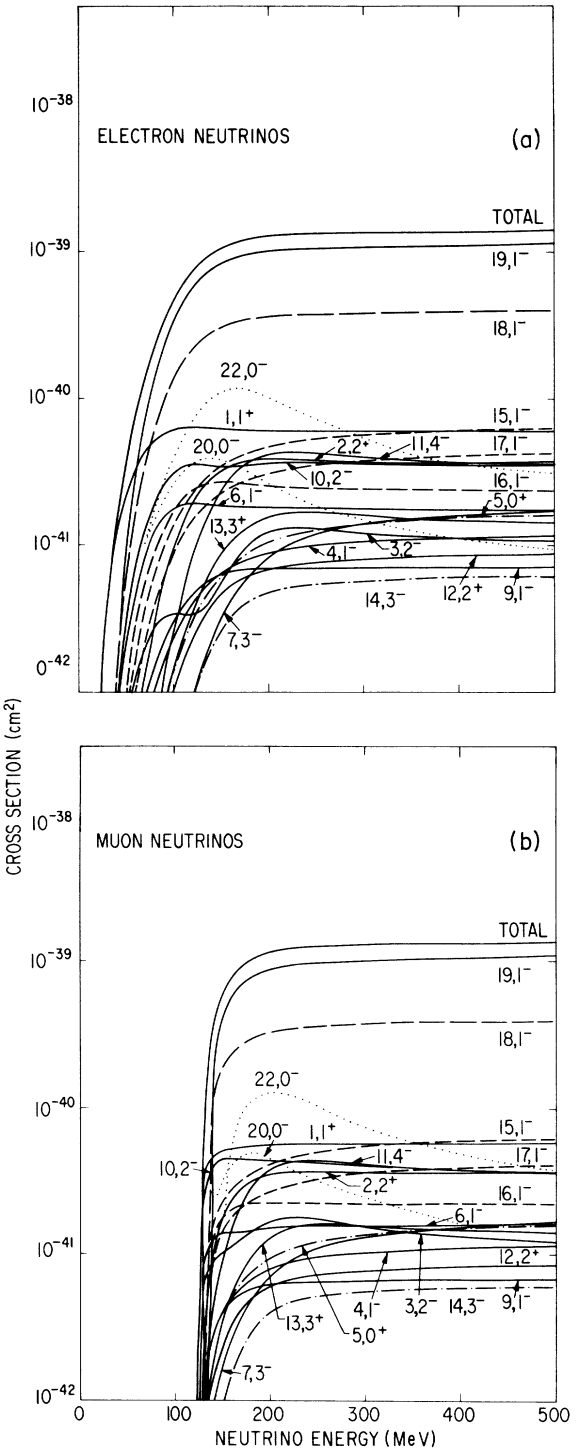

FIG. 8. Calculated ν_e and ν_μ cross sections, (a) for $\nu_e \rightarrow e$, (b) for $\nu_\mu \rightarrow \mu$, for excitation of ^{12}N levels in the range of high neutrino energies. States are labeled as in Table I. Dashed curves are included in the composite state No. 19; dash-dot curves are uncertain. Dotted cross sections (0^- levels) are taken from Ref. 5. Total does not include the dashed and the dotted curves.

10, we present the electric state angular distributions: (a) the 0^+ state (No. 5), (b) the 1^- composite state No. 18 (very similar to the composite No. 19 and also to the other 1^- states Nos. 15–17), and (c) the 3^- state (No. 14). In all cases, the peak shifts to increasingly smaller angles with increasing energy, but the 1^+ state is the only level whose angular distribution reaches all the way down to 0°.

V. SUMMARY

In this calculation, we predict the neutrino cross section of ^{12}C with the excitation of all known $T=1$ levels, mainly as observed in electron scattering. The weak transition densities were determined phenomenologically from those of electron scattering, by fitting the latter ones to the observed form factors of the levels. In this way, we expect our neutrino cross sections to be reliable and as model-independent as possible. A comparison of the in-

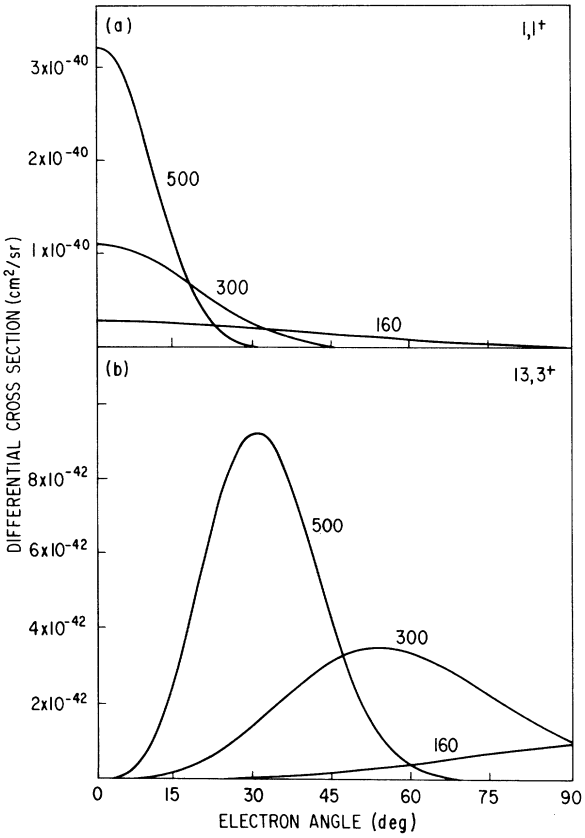

FIG. 9. Angular distributions of electrons emitted in reactions (1a) for ^{12}N magnetic states: (a) 1^+ (No. 1), (b) 3^+ (No. 13). Curves are labeled by the neutrino energy (in MeV).

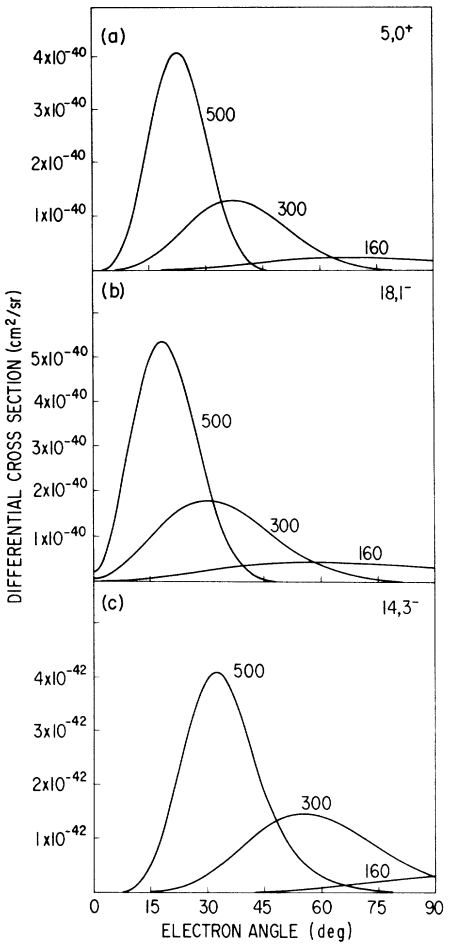

FIG. 10. Angular distributions of electrons emitted in reaction (1a) for ^{12}N electric states: (a) 0^+ (No. 5), (b) 1^- (No. 18), (c) 3^- (No. 14). Curves are labeled by neutrino energy (in MeV).

dividual cross sections with those calculated by us previously[5,6] on the basis of the particle-hole model gives the right order of magnitude of corresponding states, but some quite significant numerical differences in some states.

As to the antineutrino reaction, Eq. (2b), one sees from Eqs. (20) that the interference terms which differed in sign between neutrinos and antineutrinos have cancelled out. Therefore, except for small effects caused by differences in threshold energies, the antineutrino cross sections will be the same as those calculated in the present paper for neutrinos.

Note added in proof: After this paper had been submitted for publication, we received a report by O'Connell, Donnelly, and Walecka (ODW), since published,[38] in which the problem is treated on the basis of a particle-hole shell model. Comparison shows that as a function of E_ν, the total cross sections given by the shell model reach a maximum around 250 MeV and then descend to their asymptotic limit already at 200 MeV from below. (A similar behavior is noticeable in Fig. 4 of Ref. 5). The asymptotic limits of both models come out about the same if ODW cross sections are reduced by the phenomenological factor 2 (or 4 for the positive-parity states) mentioned by him. Excitation strengths of individual states are plotted by ODW at their cross-section maximum of $E_\nu = 250$ MeV only, and thus appear somewhat larger than our states at that energy.

ACKNOWLEDGMENTS

We wish to thank Professor C. L. Cowan and Professor F. Reines for stimulating and encouraging this investigation. We also appreciate some helpful correspondence with Professor R. Leonardi.

*Also Consultant, U. S. Naval Research Laboratory, Washington, D. C. 20390.

†Work supported in part by a grant of the National Science Foundation.

[1]H. Überall, Phys. Rev. 126, 876 (1962).

[2]H. Überall, Nuovo Cimento 41B, 25 (1966); Nuovo Cimento (Suppl.) 4, 781 (1966).

[3]See, e.g., H. Überall, *Electron Scattering from Complex Nuclei* (Academic, New York, 1971), Part B.

[4]H. Überall, Phys. Rev. 137, B502 (1965).

[5]F. J. Kelly and H. Überall, Phys. Rev. 158, 987 (1967).

[6]F. J. Kelly and H. Überall, Phys. Rev. C 5, 1432 (1972).

[7]H. Überall, Phys. Rev. 126, 1572 (1962).

[8]B. Goulard and H. Primakoff, Phys. Rev. 135, B1139 (1964).

[9]J. S. Bell and C. H. Llewellyn Smith, Nucl. Phys. B28, 317 (1971).

[10]R. A. Smith and E. J. Moniz, Stanford University Report No. ITP-395, 1971. (unpublished).

[11]F. Cannata and R. Leonardi, Phys. Rev. C 5, 1189 (1972).

[12]H. Überall, Nuovo Cimento 23, 219 (1962).

[13]K. Lande, D. C. Potter, F. Reines, H. Chen, W. R. Kropp, C. Cowan, H. Überall, R. Davis, E. Fenyves, E. Fowler, H. Frauenfelder, V. Hughes, P. Nemethy, S. L. Meyer, R. L. Burman, D. R. F. Cochran, and D. Nagle, Los Alamos Scientific Laboratory Report No. LA-4842-MS, 1971. (unpublished).

[14]See, e.g., T. W. Donnelly, J. D. Walecka, I. Sick, and E. B. Hughes, Phys. Rev. Letters 21, 1196 (1968).

[15]M. Rosen, R. Raphael, and H. Überall, Phys. Rev. 163, 927 (1967).

[16]A similar calculation is now being performed by us for the nucleus ^{16}O.

[17]Relativistic nucleon effects in weak interactions have been shown (Ref. 11) to influence only the angular distribution (in the strict forward direction), but not the total

cross section. [See also C. A. Piketty and J. Procureur, Nucl. Phys. B26, 390 (1971).]
[18]This is illustrated in Fig. 4 of Ref. 5 where total cross sections resulting from two different giant-resonance models are shown, one including the small terms, the other excluding them. The pseudoscalar is negligible for $l = e$ in any case, and for $l = \mu$ contributes noticeably ($\leq 15\%$) around $E_\nu \sim 1$ GeV only in the νn reaction, due to its additional one-pion exchange form factor [see, e.g., Y. I. Azimov and V. M. Shekhter, Soviet Phys. JETP 14, 424 (1962)]. In addition, it is shown in Ref. 11 that the pseudoscalar and weak magnetic terms can be sizable at most at large angles of the emitted lepton, but are small near forward angles. Since the angular distributions are strongly forward peaked at high energies, the effect of the small terms on the total cross sections should by negligible here.
[19]H. Überall and P. Ugin̆cius, Phys. Rev. 178, 1565 (1969).
[20]S. S. Hanna, in *Isospin in Nuclear Physics*, edited by D. H. Wilkinson (North-Holland, Amsterdam, 1969).
[21]G. A. Proca and D. B. Isabelle, Nucl. Phys. A109, 177 (1968).
[22]A. Yamaguchi, T. Terasawa, K. Nakahara, and Y. Torizuka, Phys. Rev. C 3, 1750 (1971).
[23]R. E. Segel, S. S. Hanna, and R. G. Allas, Phys. Rev. 139, B818 (1965).
[24]V. Gillet and N. Vinh-Mau, Nucl. Phys. 54, 321 (1964).
[25]F. Ajzenberg-Selove and T. Lauritsen, Nucl. Phys. A114, 1 (1968).
[26]The Helm-model fit in Ref. 15 is superseded by the present fit for which data up to much higher values of q has become available.
[27]H. Schmid and W. Scholz, Z. Physik 175, 310 (1965).
[28]G. R. Bishop, Phys. Letters 17, 310 (1965).
[29]G. A. Proca, Ph.D. thesis, University of Paris, 1966 (unpublished).
[30]J. W. Lightbody, Ph.D. thesis, University of Maryland, 1970 (unpublished).
[31]C. Werntz and H. Überall, Phys. Rev. 149, 762 (1966).
[32]H. L. Crannell, Phys. Rev. 148, 1107 (1966).
[33]W. Meyerhof, Phys. Rev. Letters 16, 1114 (1966).
[34]T. W. Donnelly, Phys. Rev. C 1, 833 (1970).
[35]P. Antony-Spies, P. P. Delsanto, E. Spamer, A. Goldmann, and O. Titze, Phys. Letters 31B, 632 (1970).
[36]N. Bezic, D. Brajinik, and G. Kernel, Nucl. Phys. A128, 426 (1969).
[37]The angular distribution given in Fig. 2 of Ref. 1 is in error, and is superseded by that of Fig. 6(a) of the present paper.
[38]J. S. O'Connell, T. W. Donnelly, and J. D. Walecka, Phys. Rev. C 6, 719 (1972).

PHYSICAL REVIEW C VOLUME 6, NUMBER 6 DECEMBER 1972

Comparison of Impulse-Approximation and Elementary-Particle Treatments in Nuclear β Decay*

Lloyd Armstrong, Jr., and C. W. Kim
Department of Physics, The Johns Hopkins University, Baltimore, Maryland 21218
(Received 15 June 1972)

We have compared the usual impulse-approximation and the elementary-particle treatments of nuclear processes using nuclear β decays as examples. Both treatments are shown to lead to essentially equivalent results for allowed transitions and for natural-parity forbidden transition of the types $\Delta J^{P_i P_f} = 1^-$ and possibly $2^+, 3^-, \ldots$. There exist, however, some differences in detailed structures in small correction terms. In the case of unnatural-parity forbidden transitions, in particular, $J_i^{P_i}(0^-) \rightarrow J_f^{P_f}(0^+) + e^- + \bar{\nu}_e$, there exist some discrepancies between the two approaches, suggesting an important role of meson-exchange corrections in the impulse approximation.

I. INTRODUCTION

There are two alternative methods used to describe nuclear weak processes such as nuclear β decay and muon capture in nuclei. The first method is to apply the usual impulse-approximation treatment (IAT); the second[1] is to treat the nuclei as "elementary particles" (EPT). The first method involves the use of model-inspired nuclear wave functions and various other approximations such as the neglect of meson-exchange and nucleon off-mass-shell effects. The second method involves, in principle, no approximation. The nuclear structure, in this case, is contained in nuclear form factors.

The two approaches are complementary in the sense that IAT is appropriate for the study of nuclear models and structures, and EPT is convenient for the study of basic ideas in weak interactions such as the conserved-vector-current (CVC) and the partially-conserved-axial-vector current (PCAC) hypotheses. In view of the fact that IAT involves the above-mentioned approximations, the use of IAT is expected to be somewhat limited, in particular in the treatment of forbidden transitions where meson-exchange cor-